Available online at www.sciencedirect.com
SCIENCE DIRECT®
Journal of Computational Physics 206 (2005) 432–452
JOURNAL OF COMPUTATIONAL PHYSICS
www.elsevier.com/locate/jcp

Monitoring energy drift with shadow Hamiltonians

Robert D. Engle, Robert D. Skeel *, Matthew Drees

Department of Computer Science, University of Illinois, 201 North Goodwin Avenue, Urbana, IL 61801-2302, USA

Received 12 July 2004; received in revised form 13 December 2004; accepted 17 December 2004
Available online 25 January 2005

Abstract

The application of a symplectic integrator to a Hamiltonian system formally conserves the value of a modified, or shadow, Hamiltonian defined by some asymptotic expansion in powers of the step size. An earlier article describes how it is possible to construct highly accurate shadow Hamiltonian approximations using information readily available from the numerical integration. This article improves on this construction by giving formulas of order up to 24 (not just up to 8) and by greatly reducing both storage requirements and roundoff error. More significantly, these high order formulas yield remarkable results not evident for 8th order formulas, even for systems as complex as the molecular dynamics of water. These numerical experiments not only illuminate theoretical properties of shadow Hamiltonians but also give practical information about the accuracy of a simulation. By removing systematic energy fluctuations, they reveal the rate of energy drift for a given step size and uncover the ill effects of using switching functions that do not have enough smoothness.

PACS: 02.60.Lj; 02.70.Ns; 05.45.Pq
Keywords: Symplectic; Hamiltonian; Modified equation; Integrator; Backward error; Numerical

1. Introduction

For the numerical solution of Hamiltonian systems of ordinary differential equations, it is common to monitor energy conservation as a check on accuracy. Due to the finite step size of a numerical integrator, it is normal for the total energy to fluctuate systematically on a short time scale and to drift randomly with

* Corresponding author. Present address: Department of Computer Sciences, Purdue University, 250 North University Street, West Lafayette, IN 47907-2066, USA. Tel.: +1 765 494 9025; fax: +1 765 494 0739.
E-mail addresses: robert@robertengle.org (R.D. Engle), skeel@cs.purdue.edu, skeel@cs.uiuc.edu (R.D. Skeel), drees@uiuc.edu (M. Drees).
URL: http://bionum.cs.purdue.edu.

0021-9991/$ - see front matter © 2005 Published by Elsevier Inc.
doi:10.1016/j.jcp.2004.12.009

an upward bias on a very long time scale. Both the fluctuations and the random drift are acceptable if sufficiently small. Unfortunately, unacceptably large random drift can be obscured by the fluctuations until a significant fraction of the simulation has been performed. Indeed, a molecular dynamics (MD) simulation may run on a computer for days before (unacceptable) energy drift can be observed. Somewhat remarkably there is another similar quantity that is much better conserved – indeed, 100,000 times better for typical MD simulations. This modified or *shadow Hamiltonian* [1] is a result of applying a particular style of backward error analysis to numerical integrators; see [2] and references therein. Moreover, an eminently practical construction for the shadow Hamiltonian is available [3]. The contribution of this work is to present a much more accurate and more efficient implementation and to report some very interesting experimental findings. In particular, these findings confirm the utility of the theory and affirm the robustness of shadow Hamiltonians. In addition, these high accuracy shadow Hamiltonians are an excellent diagnostic tool for assessing the impact of finite step size and of computational artifacts such as switching functions.

A Hamiltonian system has the form

$$\dot{x} = JH_x(x), \quad J = \begin{bmatrix} 0 & I \\ -I & 0 \end{bmatrix},$$

where the Hamiltonian $H(x)$ is a scalar function of position q and conjugate momenta p, represented collectively as $x = [q^{\mathrm{T}} p^{\mathrm{T}}]^{\mathrm{T}}$, and where the subscript x denotes differentiation.

Solving such Hamiltonian systems of equations numerically yields an approximate solution at discrete points in time separated by an amount h, with an integrator Φ_h evolving values $x^n \approx x(nh)$ at each step as $x^{n+1} = \Phi_h(x^n)$. An example of a numerical integrator is the leapfrog method which, for a separable Hamiltonian $H(q,p) = \frac{1}{2}p^{\mathrm{T}}M^{-1}p + U(q)$ with M a diagonal mass matrix and $U(q)$ the potential energy function, defines the values q^{n+1}, p^{n+1} ($,F^{n+1}$) in terms of the values q^n,p^n ($,F^n$) by:

$$p^{n+1/2} = p^n + \tfrac{1}{2}hF^n,$$

$$q^{n+1} = q^n + hM^{-1}p^{n+1/2},$$

$$F^{n+1} = -U_q(q^{n+1}),$$

$$p^{n+1} = p^{n+1/2} + \tfrac{1}{2}hF^{n+1}.$$

This formulation of the leapfrog method is often called velocity Verlet.

Generally, the most fruitful way to analyze the accuracy of a discrete approximation to a dynamical system is to express the effect of discretization as a modification to the right-hand side vector field. Such a modified, or shadow, vector field can be expressed uniquely as a formal expansion in powers of the step size. The asymptotic series converges for constant coefficient linear ordinary differential equations (for small enough step size) but generally does not converge in the nonlinear case. There is a proof of nonconvergence in [4] for the shadow vector field for the Euler method applied to $\dot{x} = x^2$. Nonetheless, a truncated expansion very accurately represents many features of the discrete dynamics.

For a Hamiltonian system, the shadow vector field is that of a Hamiltonian system if and only if the integrator is symplectic. An integrator Φ_h is *symplectic* if

$$\Phi_{h,x}(x)^{\mathrm{T}} J \Phi_{h,x}(x) = J.$$

[1] The use of the more descriptive term "shadow" rather than "modified" is suggested in [1]. The notion of a shadow Hamiltonian is different from the theory of shadowing in dynamical systems, which asserts the existence of a nearby trajectory.

The leapfrog method is an example of a symplectic integrator. If Φ_h is symplectic, the numerical trajectory $\{x^n\}$ is, therefore, *formally* the solution of a Hamiltonian system with Hamiltonian

$$H^h(x) = H(x) + h\eta_1(x) + h^2\eta_2(x) + \cdots$$

For the analytical solution, the Hamiltonian is a conserved quantity. For the numerical solution, it can be shown [5,2] that there exists $k = k(h)$ for which

$$H_{(k)}(x^n) - H_{(k)}(x^0) = \mathcal{O}(\mathrm{e}^{-c/h}) \quad \text{for time } nh \leqslant \mathrm{e}^{c/h},$$

where $H_{(k)}(x)$ = truncation of $H^h(x)$ just before the h^k term. A nice numerical example of the exponentially small error in conservation of the shadow Hamiltonian is given in [6]. However, because of the exponential growth of trajectory errors with the length t of the time interval under consideration, the analytical trajectory $x^h(t)$ for the Hamiltonian system with Hamiltonian $H_{(k)}(x)$ satisfies

$$x^h(nh) - x^n = \mathcal{O}(\mathrm{e}^{-c/h}) \quad \text{for time } nh \leqslant c/h \text{ only},$$

which for MD is not very long at all.

The truncated shadow Hamiltonian (TSH) $H_{(k)}$ involves analytical derivatives of H and is expensive to compute. Nonetheless, it is possible to construct highly accurate shadow Hamiltonian approximations using information readily available from the numerical integration. Such a possibility is presented in [3], yielding an *interpolated shadow Hamiltonian* (ISH). The idea of the construction is to extend phase space so that the new Hamiltonian $\bar{H}(y)$ is homogeneous of degree 2 and to use the fact that for such a Hamiltonian $\bar{H}(y(t)) = \frac{1}{2}\dot{y}(t)^{\mathrm{T}} J y(t)$, which enables $\bar{H}(y)$ and hence $H(x)$ to be evaluated from a trajectory. The construction of these interpolated shadow Hamiltonians assumes that the integrator is obtained by splitting the Hamiltonian, but otherwise is nearly independent of the details of the Hamiltonian system or the integrator, enabling their calculation even for systems for which the truncated shadow Hamiltonians are impractical or impossible to compute. The degree k of polynomial interpolant used in this construction determines the order of accuracy $2k$ of the resulting interpolated shadow Hamiltonian $H_{[2k]}$, so that

$$H_{[2k]}(x) = H^h(x) + \mathcal{O}(h^{2k}).$$

Concise but complete details are given in Section 4. Another, more direct but less systematic, approach to practical construction of shadow Hamiltonians is illustrated in [7] for the leapfrog method.

Remarkable results are obtained from interpolated shadow Hamiltonians with accuracy order as high as 24 and applied to systems as complex as the molecular dynamics of water. Interesting results are obtained also for truncated shadow Hamiltonians with accuracy order as high as 12 and applied to systems as complex as the two-dimensional Hénon–Heiles Hamiltonian.

As shown in Section 2, these experiments shed light on theoretical properties of shadow Hamiltonians. They indicate that the *conservation* of the truncated and interpolated shadow Hamiltonians *gets only better as the order increases* and that this is true even for a Hamiltonian that is only C^1. The range of fluctuations for the shadow Hamiltonian in the limit of high order depends on the smoothness of the potential, being smaller for smoother potentials. For the limit of small step size, exponential convergence is observed for molecular dynamics of water. Comparisons between truncated and interpolated shadow Hamiltonians for simple one- and two-dimensional potentials show that conservation of interpolated shadow Hamiltonians is somewhat inferior to that of truncated shadow Hamiltonians of the same order for sufficiently high orders.

Section 3 shows that these experiments also give practical information about the accuracy of a simulation. A relatively short computation can reveal the rate of energy drift as a function of step size. In one study, a simulation using one-sided harmonic restraints to contain molecules to a sphere exhibits occasional sudden jumps in the interpolated shadow Hamiltonians that are many orders of magnitude greater than the typical fluctuations. These large scale jumps coincide with collisions with the containing walls, events not

visible in plots of the energy alone. Other simulations reveal the ill effects of using switching functions that do not have enough smoothness, and still others explore the benefit of multiple time stepping.

Section 5 gives details of the implementation of shadow Hamiltonians. It is improved from that in [3] in three respects: (i) coefficients are given for formulas of order up to 24 not just up to 8; (ii) these formulas are revised to employ much more storage-efficient backward differences instead of centered differences; (iii) the revised algorithm reduces roundoff error by a direct calculation of first and second order backward differences that avoids blatant instances of cancellation. Concerning the value of very high order, there are cases where at least 20th order is needed to observe the behavior of the shadow Hamiltonian.

The coefficients for calculating interpolated shadow Hamiltonians up to order 24 are given in Appendix B. These formulas are also available at URL http://bionum.cs.purdue.edu/hamiltonian in the form of C code that forms part of the Hamiltonian solver used to obtain the results of this paper for systems other than MD.

2. Theoretical studies

The first four subsections consider how well the shadow energy is conserved and the fifth considers trajectory accuracy. Conservation is measured as the range $\max_n H^h_{2k}(x^n) - \min_n H^h_{2k}(x^n)$, where the $H^h_{2k}(x^n)$ are the values of the given shadow Hamiltonian at time steps $\lceil k/2 \rceil, \lceil k/2 \rceil + 1, \ldots, n_{\text{steps}} - \lceil k/2 \rceil$ with n_{steps} the total number of time steps in the simulation.

2.1. Comparison between truncated and interpolated shadow Hamiltonians

Here the truncated and the interpolated shadow Hamiltonians are compared on the basis of which is better conserved by the numerical solution. Section 2.5 considers how well analytical solutions of each of the shadow Hamiltonian equations of motion track numerical trajectories. Both sets of experiments show that the interpolated shadow Hamiltonian does not quite as well capture the numerics as does the truncated shadow Hamiltonian.

The first test problem is a one-dimensional double well potential $H(q,p) = \frac{1}{2}p^2 + \frac{1}{4}(q^2-1)^2$ with initial values $q(0) = 0$, $p(0) = 0.2$.

The second test problem is the two-dimensional Hénon–Heiles Hamiltonian

$$H(q,p) = \tfrac{1}{2}(p_1^2 + p_2^2) + \tfrac{1}{2}(q_1^2 + q_2^2 + 2q_1^2 q_2 - \tfrac{2}{3}q_2^3),$$

in which the first term represents kinetic energy and the second term represents potential energy $U(q)$ with $q = [q_1,q_2]^{\mathrm{T}}$ and $p = [p_1,p_2]^{\mathrm{T}}$. This system exhibits chaotic behavior for energies higher than 1/12, which is the case for the initial values of $q_1(0) = 1/2$, $q_2(0) = p_1(0) = p_2(0) = 0$ used in this study.

For simple potentials such as the double well or Hénon–Heiles, it is possible to obtain expressions for the lower order truncated shadow Hamiltonians. This allows for comparisons to be made between these quantities and the interpolated shadow Hamiltonians of corresponding orders. Truncated shadow Hamiltonians are obtained by using *Mathematica* to form interpolated shadow Hamiltonians $H_{[2k]}$ and to gather terms in powers of the step size h. These expressions are then truncated at the appropriate power of h to yield the desired truncated shadow Hamiltonian. Correctness is checked by comparing these results to shadow equations obtained symbolically from first principles.

We compared the two approximate shadow Hamiltonians for both the double well potential and Hénon–Heiles Hamiltonian for a variety of step sizes. Consistently it is observed that the interpolated shadow Hamiltonian is better conserved for lower orders – probably due to the exact conservation property of the ISH for quadratic Hamiltonians [3] – but as the order gets higher, the truncated shadow Hamiltonian is better conserved. The ultimate superiority of the truncated shadow Hamiltonian over interpolated shadow

Hamiltonian is clearly shown in Fig. 1, which plots energy range vs. order $2k$ for the double well potential for duration 1000 time units and $h = 0.3$, with both the truncated shadow Hamiltonian (TSH) and the interpolated shadow Hamiltonian on same semi-log plot. Truncated shadow Hamiltonian conservation data are plotted as asterisks connected by solid lines, and interpolated shadow Hamiltonian conservation data are plotted as open circles connected by dotted lines. Fig. 2 does the same for Hénon–Heiles Hamiltonian for duration 1000 time units and step size 0.9, again with both interpolated and truncated shadow Hamiltonian on same plot. The interpolatory shadow Hamiltonians do relatively better here because they are exact for quadratic Hamiltonians unlike any of the truncated shadow Hamiltonians, and Hénon–Heiles Hamiltonian is more nearly quadratic than the double well potential. The number of lower orders for which the interpolated shadow Hamiltonians are better conserved than the truncated ones is observed to decrease as the step size decreases.

2.2. Convergence

Numerical results for the double well potential and Hénon–Heiles Hamiltonian for various step sizes are consistent with the belief that truncated shadow Hamiltonians do not converge as the order goes to infinity. Nonetheless, these experiments strongly suggest that *accuracy gets only better with increasing order*. The result which best illustrates limited convergence is shown in Fig. 2, which is a plot of energy range vs. order $2k$ for Hénon–Heiles potential for $h = 0.9$. (Instability occurs for h just greater than 0.93.) The beginnings of a leveling off are also apparent in the same type of plot for the double well potential with $h = 0.5$.

Convergence is also investigated, but only for interpolated shadow Hamiltonians, for the molecular dynamics of a system of 125 water molecules whose atoms interact via bonded forces, acting among atoms within the same molecule, and nonbonded forces, acting between all intermolecular atom pairs. See Appendix A.2 for complete details.

The system of water molecules is simulated with a variety of step sizes and interpolated shadow Hamiltonians up to 24th order are evaluated. Fig. 3 shows the ISH range (in kcal/mol) vs. order $2k$ for both $h = 0.5$ fs and $h = 1.0$ fs for duration 100 ps. The limiting value for large k of the range of energy fluctuations is smaller when a smaller step size h is used.

Also, Figs. 1–3 illustrate how the conservation of the interpolated shadow Hamiltonians $H_{[2k]}$ is better for even values k than for odd values.

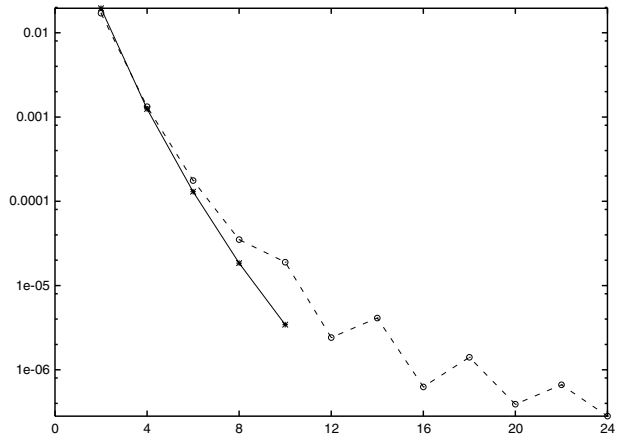

Fig. 1. Conservation of ISH (dashed) and TSH (solid) vs. order $2k$ for double well, $h = 0.3$.

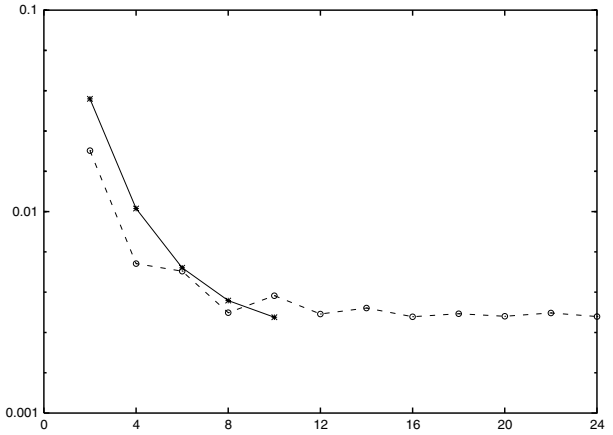

Fig. 2. Conservation of ISH (dashed) and TSH (solid) vs. order $2k$ for Hénon–Heiles, $h = 0.9$.

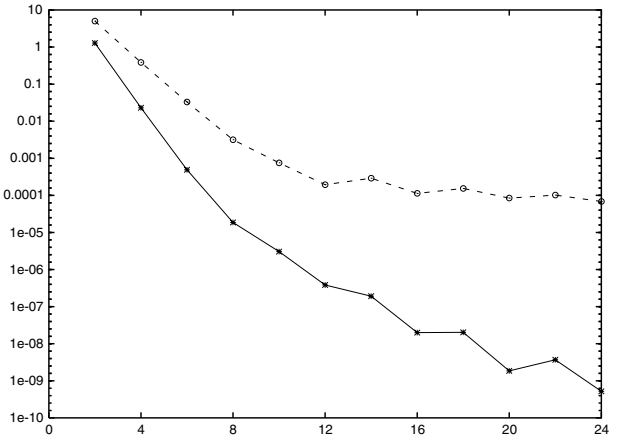

Fig. 3. Conservation of ISH vs. order $2k$ for molecular dynamics, $h = 0.5$ fs and $h = 1.0$ fs.

This dependence on k being even or odd arises because the construction of interpolated shadow Hamiltonians is somewhat different in these two cases. Nonetheless, the conservation of $H_{[2k+4]}$ is always superior to that of $H_{[2k]}$.

2.3. Smoothness needed

The fourth test problem has a one-dimensional C^1 continuous piecewise potential,

$$H(q,p) = \frac{1}{2}p^2 + U(q), \quad U(q) = \begin{cases} \frac{1}{2}q^2, & q \leqslant 0, \\ 0, & 0 \leqslant q \leqslant 6, \\ \frac{1}{2}(q-6)^2, & q \geqslant 6 \end{cases}$$

with initial conditions $q(0) = 0$, $p(0) = \sqrt{8}$.

As shown in [8, Figs. B.5 and B.6], the lack of smoothness in the piecewise potential has a clearly deleterious effect on the conservation of interpolated shadow Hamiltonians. The limiting value of the

fluctuations of these shadow Hamiltonians is much larger relative to the conservation of the actual energy than for other, smoother potentials. With $h = 0.05$ and a duration of 10,000 time units, the energy has a variation of about 0.0065 and this decreases for ISHs as the order increases leveling off at about 0.0041. Larger step sizes yield ever smaller decreases in energy fluctuations.

The energy in these simulations appears to remain bounded for all time even though the map Φ_h has jumps in its 1st derivative. An extension of the Moser twist theorem guarantees conservation of energy for maps $\Phi_h \in C^\ell$ for $\ell > 3$ [9]. This is conjectured to hold for $\ell > 2$ and counterexamples are known for $\ell = 1$.

The fifth test problem is a molecular dynamics simulation of water in which the switching distance for Lennard-Jones potential is set to be just 4 Å, which is small enough that the potential is only C^1 continuous. This again has a harmful effect on the conservation of interpolated shadow Hamiltonians. In fact, for a 10 ps simulation with step size 0.25 fs the conservation of the 24th order interpolated shadow Hamiltonian is ≈3.5 times worse than when Lennard-Jones potential is infinitely differentiable.

The cases of the C^1 continuous piecewise quadratic potential given previously and molecular dynamics with a switching distance of 4 Å stand alone among the potentials used in this study in that they are not infinitely differentiable. Both highlight one of the benefits of the construction of interpolated shadow Hamiltonians, namely the independence of that construction from many of the details of the Hamiltonian system to be solved.

2.4. Exponential convergence

Theoretically, the limiting value of the fluctuation range of the shadow Hamiltonian as a function of step size h behaves as $\exp(-c/h)$ for some constant c. Fig. 4 plots the energy range for the 24th order interpolated shadow Hamiltonian for a 100 ps simulation of water vs. $1/h$ for $h =$ 0.25, 0.5, 0.75, 1.0, 1.25, 1.5. This agrees very well with theory until the roundoff error level is reached. With a step size $h = 0.25$ fs the interpolated shadow Hamiltonian varies only in the 13th decimal digit over the length of the simulation. That this variation is due to roundoff error is suggested both by the very small magnitude of the fluctuations and by the fact that the conservation of the interpolated shadow Hamiltonian actually becomes worse when the step size is reduced from 0.25 to 0.125 fs. (The fluctuations are at the level of 15,000 U of roundoff error, which is consistent with the error accumulation and the cancellation that might be expected. The fluctuations for the double well potential are 400 U of roundoff and for Hénon–Heiles Hamiltonian 80 U.)

Similar results are obtained for the double well potential, but results for Hénon–Heiles Hamiltonian are less convincing.

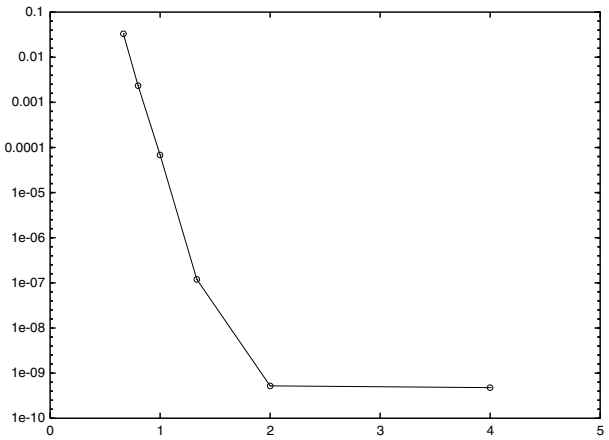

Fig. 4. Conservation of 24th order ISH vs. $1/h$ for molecular dynamics.

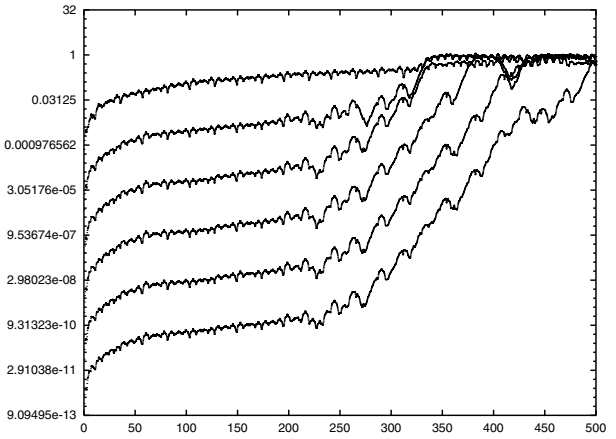

Fig. 5. Trajectory discrepancy vs. time for Hénon–Heiles TSH, $h = 0.2$.

2.5. Trajectory accuracy

Another question of interest for shadow Hamiltonians is how well their trajectories track the numerical trajectory. The truncated and interpolated forms of the shadow equations were solved to high accuracy [2] to produce trajectories associated with the two different types of shadow equations for Hénon–Heiles Hamiltonian with $h = 0.2$ for a time interval of 500 time units. These trajectories were compared to the numerical trajectory calculated by the leapfrog method with a step size of 0.2 and evaluated according to the 2-norm of the discrepancy between the numerical trajectory and the shadow Hamiltonian trajectory at each step size, where the discrepancy is the difference between the two trajectories.

Fig. 5 shows the trajectory discrepancies as a function of time for the TSH for orders $2k = 2,4,\ldots,12$ for the leapfrog method with step size $h = 0.2$. The numerical trajectory fairly rapidly separates from trajectories associated with the shadow equations, both interpolated and truncated. As expected, trajectories associated with shadow equations of higher order track the numerical solution for a longer time than do trajectories associated with shadow equations of lower orders, at least up to 12th order (the limit to which this study was carried out). The relatively short time that solutions of the truncated shadow Hamiltonian system track the numerical solution is in accord with the theory, which asserts the long-time conservation of the shadow Hamiltonian but only a short-time agreement between numerical and shadow Hamiltonian trajectories.

For formulas of orders $2,4,\ldots,12$ the trajectory discrepancy is always less for the truncated shadow Hamiltonians rather than for the interpolated shadow Hamiltonians. This is shown in [8, Fig. 2.6], which plots the trajectory discrepancies for the 12th order truncated and interpolated shadow Hamiltonians.

3. Applied studies

Observing the behavior of the shadow Hamiltonian is useful in selecting algorithms and their parameters.

[2] Integration was by the 4th order Runge–Kutta method with step size $h_{RK} = 0.00015625$. An estimate of the error in the shadow Hamiltonian trajectories was found by taking the 2-norm of 1/15th the difference between the trajectory calculated with a step size of $2h_{RK}$ and the trajectory calculated with a step size of h_{RK}. The estimated error in the shadow Hamiltonian trajectories is less than 5% for both the truncated and interpolated equations over the entire length of the simulation.

3.1. Step size

Here we examine normal behavior of the ISH time series for an MD water simulation for a variety of step sizes.

Simulations of length 100 ps for step sizes of $h = \frac{1}{8}, \frac{1}{4}, \frac{1}{2}$ fs give values for the 24th order ISH whose ranges in kcal/mol are 6.1×10^{-10}, 4.8×10^{-10}, and 5.2×10^{-10}, respectively. Clearly these fluctuations are the effect of roundoff error. For larger step sizes discrete jumps become evident. Fig. 6 shows a plot of the 24th order ISH as a function of time for a 100 ps simulation for $h = 1.0$ fs. The behavior of the 24th order ISH becomes more ragged with a decided upward drift for yet larger step sizes. Fig. 7 shows a plot of the 24th order ISH for a 1 ns simulation for $h = 2.0$ fs.

3.2. Drift in argon

Liquid argon is interesting for studying integrators because the atoms interact only through a single type of pairwise potential representing both the van der Waals attraction and the hard core repulsion. See Appendix A.1 for specific force field specifications.

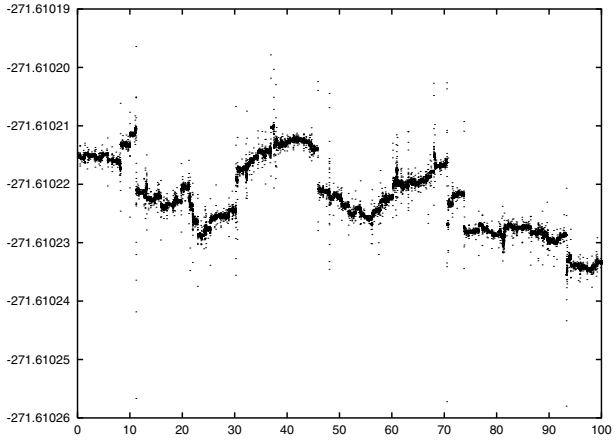

Fig. 6. 24th Order ISH for 100 ps water simulation, $h = 1.0$ fs.

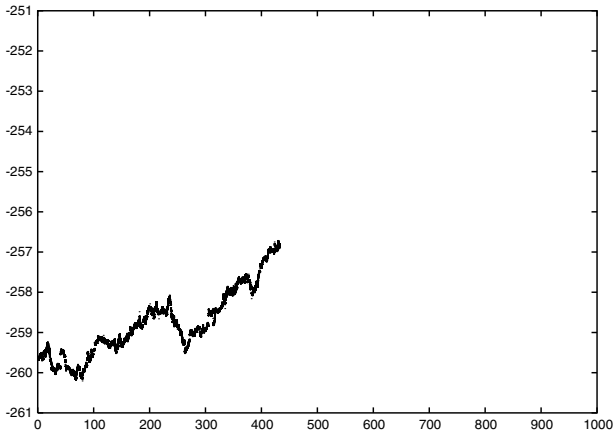

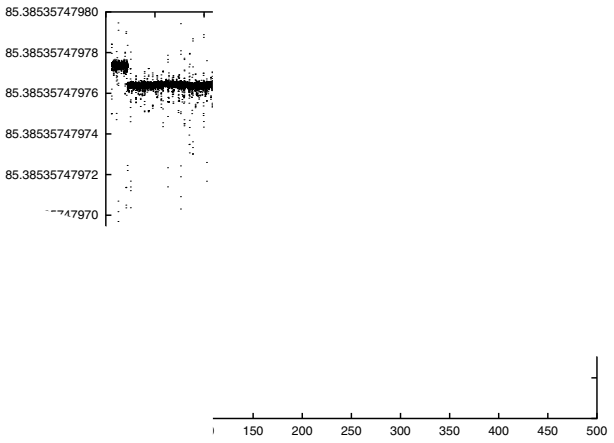

Order ISH for argon, $h = 10$ fs.

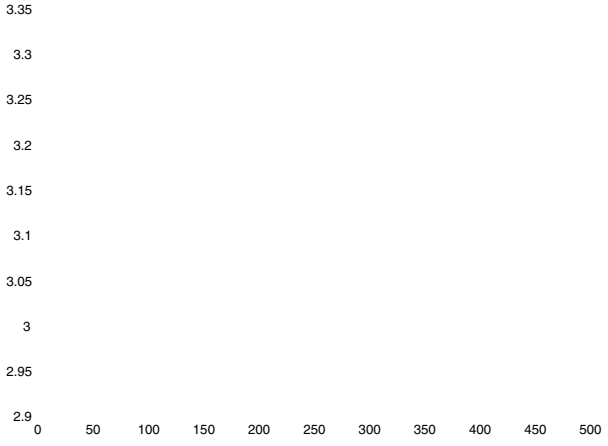

Fig. 8 shows the 24th ISH as a f time for $h = 10$ fs for a system of 250 argon atoms at 106 K. To show greater detail the vertical limited leaving the first 5 ps of simulation off the plot. Fig. 9 shows the minimum separation dista all atom pairs at each time step for that same simulation. The imes in ps when the minimum separa tance drops below 3.0 Angstroms are 5, 22, 208, 358, 394, 415, These correlate well with the tin umps in the ISH.

of restraints

der the effect of using ided harmonic restraints to contain the molecules of a water ed restraints are muc re typical for practical simulations than are the pure harmonic ests elsewhere in t article, because one-sided restraints distort the physics only at ided restraint te here is centered about the origin with the spherically symmet- e sum over a of terms

(1)

with r_i the distance from the origin to the ith atom. This potential takes effect only outside a radius of r_{BC}, and is zero for all atoms inside this radius. In this study the values $r_{BC} = 21$ Å, $k_{BC} = 1$ kcal/mol/Å^2, and $m = 2$ are used. The value $m = 2$ corresponds to the customary one-sided harmonic potential.

Plotted in Fig. 10 is the 24th order interpolated shadow Hamiltonian as a function of time for a 50 ps molecular dynamics simulation of water with step size $h = 0.5$ fs. Over the length of the simulation this shadow Hamiltonian is well conserved, with the exception of occasional sudden and clearly delineated jumps. In these instances the conservation of the interpolated shadow Hamiltonians is orders of magnitude worse for a handful of time steps before settling back down into another well conserved regime. These jumps seem to indicate some sort of event not apparent from plots of the energy or lower order interpolated shadow Hamiltonians. Further investigation determines that the jumps coincide with collisions with the soft spherical wall created by the restraints.

Accordingly, experiments were performed comparing $m = 2$ with higher values of m. The following table shows the results for water with step size $h = 1.0$ fs. The top row is the exponent m used in the boundary restraint and the bottom row is the range of the 24th order ISH:

m	2	4	6	8	10
ISH range	0.000991	0.000084	0.000024	0.000032	0.000032

Conservation is best from $m = 6$ up.

3.4. Multiple time stepping

"Impulse" multiple time stepping (MTS), most commonly known as r-RESPA, is a generalization of the leapfrog method which exploits a splitting of the potential $U = U_{fast} + U_{slow}$ so that the more costly slow part and its gradient is evaluated with a longer step size h. For example, if the fast part is evaluated twice per step, one complete step is given by:

$$p^{n+1/4} = p^n + \tfrac{1}{4}hF^n,$$

$$q^{n+1/2} = q^n + \tfrac{1}{2}hM^{-1}p^{n+1/4},$$

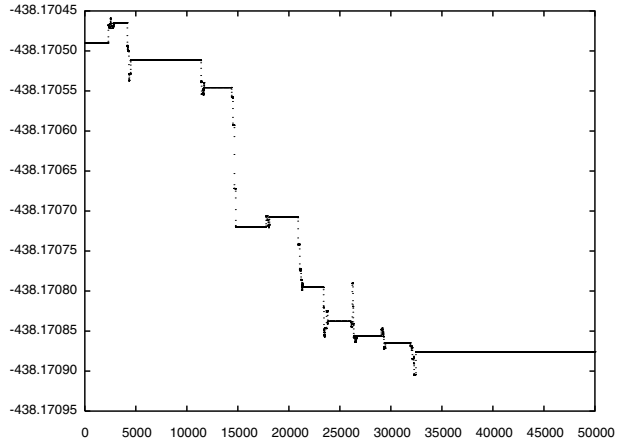

Fig. 10. 24th order ISH for 50 ps simulation of water with C^1 restraints, $h = 0.5$ fs.

$$F^{n+1/2} = -U_{\text{fast},q}(q^{n+1/2}),$$

$$p^{n+3/4} = p^{n+1/4} + \tfrac{1}{2}hF^{n+1/2},$$

$$q^{n+1} = q^{n+1/2} + \tfrac{1}{2}hM^{-1}p^{n+3/4},$$

$$F^{n+1} = -U_{\text{fast},q}(q^{n+1}) - 2U_{\text{slow},q}(q^{n+1}),$$

$$p^{n+1} = p^{n+3/4} + \tfrac{1}{4}hF^{n+1}.$$

This integrator was tested on water with the fast part consisting of the bonded forces and the boundary restraints and the slow part consisting of the nonbonded electrostatics and Lennard-Jones terms.

Tabulated below for a 100 ps simulation for three different (outer) step sizes h is the range of the 24th ISH for MTS and for leapfrog:

h	1.0	1.5	2.0
ISH range for MTS	0.000061	0.022	0.435
ISH range for leapfrog	0.000068	0.033	0.977

Given below is a similar table but for the actual energy rather than the 24th ISH:

h	1.0	1.5	2.0
Energy range for MTS	2.022	4.852	8.858
Energy range for leapfrog	5.716	13.362	24.981

The results validate the applicability of interpolated shadow Hamiltonians to (symplectic) MTS, although, for the given splitting, they show only a modest improvement for MTS over leapfrog.

4. Interpolated shadow Hamiltonians

The process specified here for the construction of the interpolated shadow Hamiltonian is from [3]. Its derivation assumes the existence of the shadow Hamiltonian.

4.1. Augmented integrator

For some given Hamiltonian H, let Φ_h be an integrator where one step of size h is the composition of exact h-flows for Hamiltonians $H_1 + H_2 + \cdots + H_L = H$. Assume that each Hamiltonian $H_l(x)$ is sufficiently smooth on some domain containing the infinite time trajectory. For instance, for a separable Hamiltonian system with $H(q,p) = \frac{1}{2}p^{\mathrm{T}}M^{-1}p + U(q)$ the leapfrog method has $L = 3$ and $H_1(x) = \frac{1}{2}U(q)$, $H_2(x) = \frac{1}{2}p^{\mathrm{T}}M^{-1}p$, and $H_3(x) = \frac{1}{2}U(q)$. Define the homogeneous extension of a Hamiltonian by

$$\bar{H}(q,\alpha,p,\beta) \stackrel{\text{def}}{=} \alpha^2 H(\alpha^{-1}q, \alpha^{-1}p)$$

and let $y \stackrel{\text{def}}{=} [q^{\mathrm{T}}, \alpha, p^{\mathrm{T}}, \beta]^{\mathrm{T}}$. Then, as shown in [3]

$$H(x(t)) \equiv \tfrac{1}{2}\dot{y}(t)^{\mathrm{T}}\bar{J}y(t),$$

where $y(t)$ is the solution for the homogeneous extension $\bar{H}(y)$ of $H(x)$ with α initially 1 and where $\bar{J}$ is similar to J but of augmented dimension. Define the augmented method $y^{n+1} = \Psi_h(y^n)$ for $\bar{H}$ to be the composition of exact flows for systems with Hamiltonians $\bar{H}_1, \bar{H}_2, \ldots, \bar{H}_L$ where

$$\bar{H}_l(q,\alpha,p,\beta) \stackrel{\text{def}}{=} \alpha^2 H_l(\alpha^{-1}q, \alpha^{-1}p).$$

For example, the augmented leapfrog method with $\alpha^0 = 1$ is given by:

$$p^{n+1/2} = p^n + \frac{h}{2}F^n,$$

$$\beta^{n+1/2} = \beta^n + \frac{h}{2}(-(q^n)^{\mathrm{T}}F^n - 2U^n),$$

$$q^{n+1} = q^n + hM^{-1}p^{n+1/2},$$

$$F^{n+1} = F(q^{n+1}),$$

$$p^{n+1} = p^{n+1/2} + \frac{h}{2}F^{n+1},$$

$$\beta^{n+1} = \beta^{n+1/2} + \frac{h}{2}(-(q^{n+1})^{\mathrm{T}}F^{n+1} - 2U^{n+1}).$$

Let $H^h(q,p)$ be the shadow Hamiltonian of the original method Φ_h. Then it can be shown [3] that the augmented method Ψ_h has a shadow Hamiltonian

$$\bar{H}^h(q,\alpha,p,\beta) = \alpha^2 H^h(\alpha^{-1}q, \alpha^{-1}p).$$

Furthermore, let the shadow Hamiltonians H^h and $\bar{H}^h$ have solutions $x_h(t)$ and $y_h(t)$, respectively. Then it is shown in [3] that

$$H^h(x_h(t)) \equiv \tfrac{1}{2}\dot{y}_h(t)^{\mathrm{T}}\bar{J}y_h(t).$$

4.2. Construction of $H_{[2k]}$ for even k

The construction of $H_{[2k]}(q,p)$ for *even values of* k follows. See [3] for odd values of k. Given a shadow extended Hamiltonian system with initial condition $y_h(0) = [q^{\mathrm{T}},1,p^{\mathrm{T}},0]^{\mathrm{T}}$, let $y_h(t)$ be its solution with values $y_h(jh) = \Psi_h^j(y_h(0)), j = 0, \pm 1, \ldots, \pm k/2$. Let $\pi_k(t)$ be the degree k polynomial interpolant of these $k+1$ values. Following the approach of [3], let:

$$H_{k,j} \stackrel{\text{def}}{=} \frac{1}{jh}\int_{-jh/2}^{jh/2} \frac{1}{2}\dot{\pi}_k(t)^{\mathrm{T}}J\pi_k(t)\,\mathrm{d}t, \quad j = 2,4,\ldots,k.$$

As shown in [3], this has an expansion

$$H_{k,j} = H^h + c_{j1}h^{k+2}\dot{\gamma}(0) + c_{j3}h^{k+4}\dddot{\gamma}(0) + \cdots + \mathcal{O}(h^{2k+2}),$$

where

$$\gamma(t) \stackrel{\text{def}}{=} \tfrac{1}{2}\dot{y}_h(t)^{\mathrm{T}}\bar{J}y_h^{[k+1]}(t)$$

with the brackets denoting a $(k+1)$th divided difference, namely, $y_h^{[k+1]}(t) \stackrel{\text{def}}{=} y_h[-\frac{1}{2}kh, \ldots, \frac{1}{2}kh, t]$. As in [3], the first $k/2-1$ leading error terms can be eliminated by forming a suitable linear combination of the $H_{k,j}$, $j = 1,2,\ldots,k/2$, to yield

$H_{[2k]} \stackrel{\text{def}}{=}$ some linear combination of the $H_{k,j} = H^h + \mathcal{O}(h^{2k})$.

The coefficients of these linear combinations are given in Appendix B. A concrete example for the case of $k = 4$ is

$$H_{[8]}(x) = \tfrac{16}{21}H_{4,2} + \tfrac{5}{21}H_{4,4} = H^h(x) + \mathcal{O}(h^8).$$

5. A better implementation

Shadow Hamiltonians up through order 24 have been obtained and are given in Appendix B. Previously [3], only shadow Hamiltonians up through order 8 had been obtained. With the use of higher order formulas it is all the more important that the required differences be calculated with optimal storage efficiency and with minimal roundoff error.

In practice, implementation of interpolated shadow Hamiltonians $H_{[2k]}$ for odd k is unnecessary when the goal is to obtain the formulas with highest order accuracy possible, which, as this article indicates, exhibit the best conservation behavior. Implementation of only the even k case is sufficient for this purpose, and has the advantage that extra work needed to compute differences of midstep quantities is avoided. For this reason the following discussion is limited to the case of even k.

5.1. Backward difference derivation for even k

This section presents formulas for $H_{[2k]}$ for even values of k. See [8] for odd values of k. Let a_j be the jth backward difference of $y_h(t)$ at $t = (k/2)h$

$$a_j = \nabla^j y_h((k/2)h), \quad j = 0, 1, 2, \ldots, k,$$

where the backward difference is defined by $\nabla^k w(t) = \nabla^{k-1} w(t) - \nabla^{k-1} w(t-h)$, $\nabla^0 w(t) = w(t)$. Taking the case $k = 4$ as an example, the fourth degree Newton interpolant using backward differences is

$$\pi_4(t) = y_h(2h) + (t-2h)\frac{\nabla y_h(2h)}{h} + (t-2h)(t-h)\frac{\nabla^2 y_h(2h)}{2h^2} + t(t-2h)(t-h)\frac{\nabla^3 y_h(2h)}{6h^3} + t(t-2h)(t^2-h^2)\frac{\nabla^4 y_h(2h)}{24h^4}.$$

Hence

$$\pi_4(sh) = a_0 + (s-2)a_1 + \tfrac{1}{2}(s-2)(s-1)a_2 + \tfrac{1}{6}s(s-2)(s-1)a_3 + \tfrac{1}{24}s(s-2)(s^2-1)a_4$$

and

$$h\dot{\pi}_4(sh) = a_1 + \left(s - \tfrac{3}{2}\right)a_2 + \left(\tfrac{1}{2}s^2 - s + \tfrac{1}{3}\right)a_3 + \tfrac{1}{2}\left(\tfrac{1}{3}s^3 - \tfrac{1}{2}s^2 - \tfrac{1}{6}s + \tfrac{1}{6}\right)a_4.$$

Define $A_{ij} = a_i^{\mathrm{T}} \bar{J} a_j/(2h)$. Using the facts that $A_{ii} = 0$ and $A_{ij} = -A_{ji}$, this yields

$$\begin{aligned}\tfrac{1}{2}\dot{\pi}_4(sh)^{\mathrm{T}}\bar{J}\pi_4(sh) = {} & A_{10} - \tfrac{3}{2}A_{20} + \left(2 + \tfrac{1}{2}s^2\right)A_{21} + \left(\tfrac{1}{3} + \tfrac{1}{2}s^2\right)A_{30} - \left(\tfrac{2}{3} + \tfrac{3}{2}s^2\right)A_{31} + \left(\tfrac{1}{3} + \tfrac{13}{12}s^2 + \tfrac{1}{12}s^4\right)A_{32} \\ & + \left(\tfrac{1}{12} - \tfrac{1}{4}s^2\right)A_{40} + \left(-\tfrac{1}{6} + \tfrac{11}{24}s^2 + \tfrac{1}{8}s^4\right)A_{41} + \left(\tfrac{1}{12} - \tfrac{11}{48}s^2 - \tfrac{11}{48}s^4\right)A_{42} \\ & + \left(\tfrac{1}{36}s^2 + \tfrac{13}{144}s^4 + \tfrac{1}{144}s^6\right)A_{43} + \text{odd powers of } s.\end{aligned}$$

Average over $-1 \leqslant s \leqslant 1$ to obtain $H_{4,2}$ and over $-2 \leqslant s \leqslant 2$ to obtain $H_{4,4}$, as

$$H_{4,2} = \frac{1}{2}\int_{-1}^{1} \frac{1}{2}\dot{\pi}_4(sh)^{\mathrm{T}}\bar{J}\pi_4(sh)\,\mathrm{d}s \quad \text{and} \quad H_{4,4} = \frac{1}{4}\int_{-2}^{2} \frac{1}{2}\dot{\pi}_4(sh)^{\mathrm{T}}\bar{J}\pi_4(sh)\,\mathrm{d}s.$$

From this one finds

$$H_{[8]} = \tfrac{16}{21}H_{4,2} + \tfrac{5}{21}H_{4,4} = A_{10} - \tfrac{3}{2}A_{20} + \tfrac{16}{7}A_{21} + \tfrac{13}{21}A_{30} - \tfrac{32}{21}A_{31} + \tfrac{36}{35}A_{32} - \tfrac{5}{84}A_{40} + \tfrac{22}{105}A_{41} - \tfrac{9}{35}A_{42} + \tfrac{4}{35}A_{43}.$$

This and other formulas in terms of the A_{ij} for $H_{[2k]}$ with k even can be found in Appendix B.

5.2. Storage considerations

The efficiency of the construction of interpolated shadow Hamiltonians as presented in [3] and reviewed in Section 4 derives from the fact that the interpolated shadow Hamiltonians $H_{[2k]}$ are built from consecutive solution values $y^{n-k/2}$, $y^{n-k/2+1}, \ldots, y^{n+k/2-1}, y^{n+k/2}$, values which are already being calculated by the simulation. Differences of these values are formed that represent the interpolants, and these differences are used to construct the interpolated shadow Hamiltonians. The introduction of these differences of solution values requires additional storage beyond what is necessary for the simulation alone, because these differences must be stored. The scheme given in [3] employs centered differences. However, the use of backward differences, as presented here, results in significant savings in storage costs. Consider the difference tables up to fourth order differences, which are required for calculating $H_{[8]}$, for both centered and backward differences. The centered difference table is

$$\begin{array}{lllll}
\delta^0 y_h(t-2h) & & & & \\
 & \delta^1 y_h(t-\frac{3}{2}h) & & & \\
\delta^0 y_h(t-h) & & \delta^2 y_h(t-h) & & \\
 & \underline{\underline{\delta^1 y_h(t-\frac{1}{2}h)}} & & \underline{\underline{\delta^3 y_h(t-\frac{1}{2}h)}} & \\
\underline{\underline{\delta^0 y_h(t)}} & & \underline{\underline{\delta^2 y_h(t)}} & & \underline{\underline{\delta^4 y_h(t)}} \\
 & \underline{\underline{\delta^1 y_h(t+\frac{1}{2}h)}} & & \underline{\underline{\delta^3 y_h(t+\frac{1}{2}h)}} & \\
\underline{\delta^0 y_h(t+h)} & & \underline{\delta^2 y_h(t+h)} & & \\
 & \underline{\delta^1 y_h(t+\frac{3}{2}h)} & & & \\
\underline{\delta^0 y_h(t+2h)} & & & &
\end{array}$$

The backward difference table is

$$\begin{array}{lllll}
\nabla^0 y_h(t-2h) & & & & \\
 & \nabla^1 y_h(t-h) & & & \\
\nabla^0 y_h(t-h) & & \nabla^2 y_h(t) & & \\
 & \nabla^1 y_h(t) & & \nabla^3 y_h(t+h) & \\
\nabla^0 y_h(t) & & \nabla^2 y_h(t+h) & & \underline{\underline{\nabla^4 y_h(t+2h)}} \\
 & \nabla^1 y_h(t+h) & & \underline{\underline{\nabla^3 y_h(t+2h)}} & \\
\nabla^0 y_h(t+h) & & \underline{\underline{\nabla^2 y_h(t+2h)}} & & \\
 & \underline{\underline{\nabla^1 y_h(t+2h)}} & & & \\
\underline{\underline{\nabla^0 y_h(t+2h)}} & & & &
\end{array}$$

Formulas for the interpolated shadow Hamiltonians are in terms of the doubly underlined values. However, for purposes of calculating these doubly underlined values, both these and the singly underlined values must be stored. Thus, to compute $H_{[8]}$ using centered differences, eleven sets of values must be stored in addition to the storage already required for the simulation, while to compute $H_{[8]}$ using backward differences only 4 additional sets of values must be stored. The 0th difference $y_h(t+2h)$ is "free", since this consists of the current values of q, p, and β.

Assuming k is even, the centered difference table requires extra storage of $\sum_{i=1}^{k/2}(2i+2) = \frac{1}{4}k^2 + \frac{3}{2}k$ vectors, while the backward difference table requires extra storage of only k. The savings are especially significant for systems with a large number of configurational degrees of freedom and for high order shadow Hamiltonians.

5.3. Rounding error considerations

Using leapfrog integration, the key backward differences of full step quantities from which higher order differences are calculated are as follows: $\nabla q^{n+1} = hM^{-1}p^{n+1/2}$, $\nabla^2 q^{n+1} = h^2 M^{-1}F^n$, calculated before the leapfrog force update; $\alpha^n = 1$, $\nabla^i \alpha^n = 0$ for $i \geqslant 0$ which need neither be stored nor computed; $\nabla p^{n+1} = \frac{1}{2}h(F^{n+1} + F^n)$, which can be calculated during the leapfrog force update so that new and old force values are available; and $\nabla \beta^{n+1} = \frac{1}{2}h(-(q^n)^{\mathrm{T}}F^n - 2U^n - (q^{n+1})^{\mathrm{T}}F^{n+1} - 2U^{n+1})$, the first part of which may be calculated before the leapfrog position update using the values q^n, F^n, U^n and the second part of which may be calculated after the leapfrog force update using the values q^{n+1}, F^{n+1}, U^{n+1}.

Using the preceding expressions, the first and second order backward differences of key full step simulation quantities are found analytically, rather than numerically. Directly calculating low order differences avoids harmful cancellation, thus avoiding unnecessary rounding error.

As before, let k determine the maximum order of shadow Hamiltonian $H_{[2k]}$ to be computed. A new row of the backward difference table consists of the values

$$\nabla^i y^{n+1} = \left[(\nabla^i q^{n+1})^{\mathrm{T}}, \nabla^i \alpha^{n+1}, (\nabla^i p^{n+1})^{\mathrm{T}}, \nabla^i \beta^{n+1}\right]^{\mathrm{T}}, \quad i = 0, 1, \ldots, k.$$

Presented in the context of a single step of the leapfrog method these updates take place as follows:

$$\nabla^2 q^{n+1} = h^2 M^{-1} F^n \quad \text{and} \quad \nabla^i q^{n+1} = \nabla^{i-1} q^{n+1} - \nabla^{i-1} q^n, \quad i = 3, 4, \ldots, k,$$

$$\nabla q^{n+1} = \nabla q^n + \nabla^2 q^{n+1},$$

$$q^{n+1} = q^n + \nabla q^{n+1},$$

$$\nabla p^{n+1}_{\mathrm{half}} = \tfrac{1}{2}hF^n,$$

$$\nabla \beta^n_{\mathrm{half}} = \frac{h}{2}(-(q^n)^{\mathrm{T}}F^n - 2U^n),$$

$$F^{n+1} = F(q^{n+1}),$$

$$\nabla p^{n+1} = \nabla p^{n+1}_{\mathrm{half}} + \tfrac{1}{2}hF^{n+1} \quad \text{and} \quad \nabla^i p^{n+1} = \nabla^{i-1} p^{n+1} - \nabla^{i-1} p^n, \quad i = 2, 3, \ldots, k,$$

$$\nabla \beta^{n+1} = \nabla \beta^n_{\mathrm{half}} + \frac{h}{2}(-(q^{n+1})^{\mathrm{T}}F^{n+1} - 2U^{n+1}) \quad \text{and} \quad \nabla^i \beta^{n+1} = \nabla^{i-1} \beta^{n+1} - \nabla^{i-1} \beta^n, \quad i = 2, 3, \ldots, k,$$

$$p^{n+1} = \frac{1}{h}M\nabla q^{n+1} + \frac{h}{2}F^{n+1}.$$

Only differences of β, not β itself, need to be computed, since only these are necessary to calculate interpolated shadow Hamiltonian formulas. This is the case because all differences of α of first order and above are zero, so terms involving 0th order differences of β drop out.

As constructed, the interpolated shadow Hamiltonians are defined by linear combinations of A_{ij} terms. As the order of interpolated shadow Hamiltonians increases, these formulas quickly become very long and impractical to code by hand. Instead, the coefficients of the A_{ij} terms in the various $H_{[2k]}$ equations can be stored in arrays initialized before integration begins and then referenced as needed, simplifying the expansion to higher values of k. See, for example, the code for a Hamiltonian solver in [8, Appendix B], which is available electronically from: http://bionum.cs.purdue.edu/hamiltonian.

Acknowledgment

This material is based upon work performed at the University of Illinois at Urbana-Champaign and supported by the National Science Foundation under Grant 020442 and by NIH Grant P41RR05969.

Appendix A. Molecular dynamics details

For molecular dynamics of a system of N atoms, the coordinate vectors q and p are each of length $3N$ and the mass matrix is diagonal with each atom mass replicated 3 times.

Molecular dynamics results are obtained using a modified version of a program [3] compatible with NAMD [10] but limited in scope to enable simpler modification. Interpolated shadow Hamiltonian code was added to this program by the first author.

A.1. Argon

The system studied consists of 250 argon atoms which interact via a nonbonded force between all atom pairs and which are spherically restrained by an artificial harmonic force. The mass of an argon atom is 39.948 amu.

The potential can be expressed as the sum of nonbonded terms and boundary restraints, where in this study the nonbonded potential is Lennard–Jones potential $U_{\mathrm{LJ}}(q)$.

The atoms are restrained to a sphere centered about the origin with the spherically symmetric potential U_{BC} equal to the sum over all i of terms $k_{\mathrm{BC}} r_i^2$, with r_i the distance from the origin to the ith atom. In this study the value $k_{\mathrm{BC}} = \frac{4}{441}$ kcal/mol/Å^2 is used to give energy equal to that of the usual one-sided quadratic restraints given by Eq. (1) at a distance of about 23 Å. The use of pure harmonic restraints rather than one-sided harmonic restraints avoids unnecessary nonsmoothness.

Lennard-Jones potential exists between all pairs of atoms, with U_{LJ} equal to the sum, over all (i,j)-pairs, of terms

$$E_{\min}\left[\left(\frac{R_{\min}}{r_{ij}}\right)^{12} - 2\left(\frac{R_{\min}}{r_{ij}}\right)^{6}\right]. \tag{A.1}$$

[3] Credit: David J. Hardy, Department of Computer Science and Beckman Institute, University of Illinois, 405 North Mathews Avenue, Urbana, IL 61801-2987 (dhardy@ks.uiuc.edu).

The minimum value of the potential $-E_{\min}$ and the equilibrium separation distance $R_{\min}$ depend on the atom types involved in the interaction. For argon–argon interactions, $E_{\min} = 0.2385$ kcal/mol and $R_{\min} = 3.4050$ Å. *Commonly in molecular dynamics simulations Lennard-Jones potential is taken to be zero outside a given cutoff distance* r_c. To achieve a smooth transition, a switching function is applied to the potential before the cutoff distance but outside some switching distance r_s, so that in this range the contribution of each intermolecular (i,j)-pair towards the total U_{LJ} becomes

$$E_{\min}\left[\left(\frac{R_{\min}}{r_{ij}}\right)^{12} - 2\left(\frac{R_{\min}}{r_{ij}}\right)^{6}\right]\left[\frac{(r_c^2 - r_{ij}^2)^2(r_c^2 + 2r_{ij}^2 - 3r_s^2)}{(r_c^2 - r_s^2)^3}\right] \quad \text{for } r_s \leqslant r_{ij} \leqslant r_c.$$

The use of this switching function results in a C^1 continuous Lennard-Jones potential. However, in this study the switching distance was chosen large enough that no switching would ever take place, due to the imposed spherical boundary restraints. Lennard-Jones potential, therefore, remains infinitely differentiable. The one exception occurs in Section 2.3, in which results from molecular dynamics with $r_s = 4$ Å, $r_c = 100$ Å are discussed.

Initial conditions are obtained by using NAMD to equilibrate to a temperature of 106 K.

A.2. Water

The system studied consists of 125 water molecules whose atoms interact via two bonded forces, acting between and among atoms within the same molecule, and two nonbonded forces, acting between all intermolecular atom pairs. Also the atoms are spherically restrained by an artificial harmonic force. The mass of a hydrogen atom is 1.0080 amu and that of an oxygen atom is 15.9994 amu.

The potential can be expressed as the sum of bonded terms, nonbonded terms, and boundary restraints, where in this study the bonded potentials are bond stretching and angle bending and the nonbonded potentials are Lennard-Jones potential and the electrostatic potential, so that

$$U(q) = U_{BC}(q) + U_{bond}(q) + U_{angle}(q) + U_{LJ}(q) + U_{elec}(q).$$

The atoms are restrained by the same boundary potential as the argon system.

The first bonded potential, the spring bond, is a 2-body interaction between pairs of covalently bonded atoms, with U_{bond} equal to the sum, over all such (i,j)-pairs, of terms $k_b(r_{ij} - r_0)^2$, with r_{ij} the separation distance of the two atoms. For the case of hydrogen–oxygen interactions, the coefficient $k_b = 450$ kcal/mol/Å^2 and the equilibrium distance $r_0 = 0.957$ Å.

The angle potential is a 3-body interaction between a consecutively bonded triples of atoms, with U_{angle} equal to the sum, over all such (i,j,k)-triples, of terms $k_\theta(\theta - \theta_0)^2$, with θ the angle in radians between the vector pointing from atom j to atom i and the vector pointing from atom j to atom k. For the case of water molecules, the coefficient $k_\theta = 55$ kcal/mol/rad^2 and the equilibrium angle $\theta_0 = 1.8242$ rad.

Lennard-Jones potential exists between all intermolecular pairs of atoms, with U_{LJ} equal to the sum, over all intermolecular (i,j)-pairs, of terms given by Eq. (A.1) where $E_{\min} = 0.046$ kcal/mol and $R_{\min} = 0.449$ Å for hydrogen–hydrogen interactions, $E_{\min} = 0.0836$ kcal/mol and $R_{\min} = 1.9927$ Å for hydrogen–oxygen interactions, and $E_{\min} = 0.1521$ kcal/mol and $R_{\min} = 3.5364$ Å for oxygen–oxygen interactions.

The electrostatic potential U_{elec} equals the sum, over all intermolecular atom (i,j)-pairs, of terms

$$\frac{CZ_iZ_j}{\varepsilon_0 r_{ij}},$$

where the quantities Z_i and Z_j are the charges of atom i and atom j, respectively. Atom charges, in units of electron charge, are 0.417 e for hydrogen and −0.834 e for oxygen bound in water molecules. The coefficient $C = 332.0636$ kcal Å/mol/e^2 is Coulomb's constant. The dielectric constant used is $\varepsilon_0 = 1$. As with Lennard-Jones potential, the electrostatic potential can be taken to be zero beyond the cutoff distance r_c with a switching function applied to the potential inside this distance, so that the contribution to U_{elec} from each intermolecular (i,j)-pair of atoms becomes

$$\frac{CZ_iZ_j}{\varepsilon_0 r_{ij}}\left(1-\frac{r_{ij}^2}{r_c^2}\right)^2 \quad \text{for } 0 < r_{ij} \leqslant r_c.$$

This results in a C^1 continuous electrostatic potential. However, in this study a cutoff $r_c = 100$ Å was chosen so that it would never be reached, thus maintaining an infinitely differentiable electrostatic potential.

Initial conditions are randomly generated by NAMD for a system at 300 K.

Appendix B. Interpolated shadow Hamiltonians up to order 24

The following formulas for shadow Hamiltonians up through order 24 are obtained using *Mathematica*:

$$H_{[2]} = H_{1,1},$$

$$H_{[4]} = H_{2,2},$$

$$H_{[6]} = \tfrac{9}{20}H_{3,1} + \tfrac{11}{20}H_{3,3},$$

$$H_{[8]} = \tfrac{16}{21}H_{4,2} + \tfrac{5}{21}H_{4,4},$$

$$H_{[10]} = \tfrac{50}{189}H_{5,1} + \tfrac{325}{504}H_{5,3} + \tfrac{137}{1512}H_{5,5},$$

$$H_{[12]} = \tfrac{25}{44}H_{6,2} + \tfrac{2}{5}H_{6,4} + \tfrac{7}{220}H_{6,6},$$

$$H_{[14]} = \tfrac{1225}{6864}H_{7,1} + \tfrac{6909}{11440}H_{7,3} + \tfrac{1421}{6864}H_{7,5} + \tfrac{11}{1040}H_{7,7},$$

$$H_{[16]} = \tfrac{1568}{3575}H_{8,2} + \tfrac{14896}{32175}H_{8,4} + \tfrac{7136}{75075}H_{8,6} + \tfrac{761}{225225}H_{8,8},$$

$$H_{[18]} = \tfrac{7938}{60775}H_{9,1} + \tfrac{32634}{60775}H_{9,3} + \tfrac{1458}{5005}H_{9,5} + \tfrac{2997}{74800}H_{9,7} + \tfrac{7129}{6806800}H_{9,9},$$

$$H_{[20]} = \tfrac{1470}{4199}H_{10,2} + \tfrac{13920}{29393}H_{10,4} + \tfrac{37665}{235144}H_{10,6} + \tfrac{4190}{264537}H_{10,8} + \tfrac{671}{2116296}H_{10,10},$$

$$H_{[22]} = \tfrac{847}{8398}H_{11,1} + \tfrac{194205}{411502}H_{11,3} + \tfrac{2247575}{6584032}H_{11,5} + \tfrac{119185}{1493856}H_{11,7} + \tfrac{588181}{98760480}H_{11,9} + \tfrac{83711}{888844320}H_{11,11},$$

$$H_{[24]} = \tfrac{104544}{364021}H_{12,2} + \tfrac{669735}{1456084}H_{12,4} + \tfrac{233530}{1092063}H_{12,6} + \tfrac{67034}{1820105}H_{12,8} + \tfrac{8614}{4004231}H_{12,10} + \tfrac{6617}{240253860}H_{12,12},$$

Below, these formulas are expressed in terms of backward differences of numerical solution values for even values of k. See [8] for odd values of k.

$$H_{[4]} = A_{1,0} - \tfrac{1}{2}A_{2,0} + \tfrac{2}{3}A_{2,1},$$

$$H_{[8]} = A_{1,0} - \tfrac{3}{2}A_{2,0} + \tfrac{16}{7}A_{2,1} + \tfrac{13}{21}A_{3,0} - \tfrac{32}{21}A_{3,1} + \tfrac{36}{35}A_{3,2} - \tfrac{5}{84}A_{4,0} + \tfrac{22}{105}A_{4,1} - \tfrac{9}{35}A_{4,2} + \tfrac{4}{35}A_{4,3},$$

$$\begin{aligned} H_{[12]} = {} & A_{1,0} - \tfrac{5}{2}A_{2,0} + \tfrac{54}{11}A_{2,1} + \tfrac{74}{33}A_{3,0} - \tfrac{72}{11}A_{3,1} + \tfrac{125}{22}A_{3,2} - \tfrac{19}{22}A_{4,0} + \tfrac{141}{44}A_{4,1} - \tfrac{375}{88}A_{4,2} + \tfrac{500}{231}A_{4,3} + \tfrac{29}{220}A_{5,0} - \tfrac{3}{5}A_{5,1} \\ & + \tfrac{325}{308}A_{5,2} - \tfrac{200}{231}A_{5,3} + \tfrac{45}{154}A_{5,4} - \tfrac{7}{1320}A_{6,0} + \tfrac{137}{4620}A_{6,1} - \tfrac{125}{1848}A_{6,2} + \tfrac{5}{63}A_{6,3} - \tfrac{15}{308}A_{6,4} + \tfrac{1}{77}A_{6,5}, \end{aligned}$$

$$\begin{aligned} H_{[16]} = {} & A_{1,0} - \tfrac{7}{2}A_{2,0} + \tfrac{128}{15}A_{2,1} + \tfrac{73}{15}A_{3,0} - \tfrac{256}{15}A_{3,1} + \tfrac{10976}{585}A_{3,2} - \tfrac{41}{12}A_{4,0} + \tfrac{1712}{117}A_{4,1} - \tfrac{2744}{117}A_{4,2} + \tfrac{10976}{715}A_{4,3} + \tfrac{743}{585}A_{5,0} \\ & - \tfrac{3712}{585}A_{5,1} + \tfrac{406112}{32175}A_{5,2} - \tfrac{43904}{3575}A_{5,3} + \tfrac{6860}{1287}A_{5,4} - \tfrac{31}{130}A_{6,0} + \tfrac{4896}{3575}A_{6,1} - \tfrac{104272}{32175}A_{6,2} + \tfrac{128968}{32175}A_{6,3} - \tfrac{3430}{1287}A_{6,4} \\ & + \tfrac{3136}{3861}A_{6,5} + \tfrac{37}{1925}A_{7,0} - \tfrac{28544}{225225}A_{7,1} + \tfrac{11368}{32175}A_{7,2} - \tfrac{1568}{2925}A_{7,3} + \tfrac{140}{297}A_{7,4} - \tfrac{896}{3861}A_{7,5} + \tfrac{112}{2145}A_{7,6} - \tfrac{761}{1801800}A_{8,0} \\ & + \tfrac{22}{6825}A_{8,1} - \tfrac{343}{32175}A_{8,2} + \tfrac{1918}{96525}A_{8,3} - \tfrac{175}{7722}A_{8,4} + \tfrac{28}{1755}A_{8,5} - \tfrac{14}{2145}A_{8,6} + \tfrac{8}{6435}A_{8,7}, \end{aligned}$$

$$\begin{aligned} \mathrm{H}_{[20]} = {} & \mathrm{A}_{1,0} - \tfrac{9}{2}\mathrm{A}_{2,0} + \tfrac{250}{19}\mathrm{A}_{2,1} + \tfrac{484}{57}\mathrm{A}_{3,0} - \tfrac{2000}{57}\mathrm{A}_{3,1} + \tfrac{30375}{646}\mathrm{A}_{3,2} - \tfrac{497}{57}\mathrm{A}_{4,0} + \tfrac{167125}{3876}\mathrm{A}_{4,1} - \tfrac{212625}{2584}\mathrm{A}_{4,2} + \tfrac{21600}{323}\mathrm{A}_{4,3} \\ & + \tfrac{34167}{6460}\mathrm{A}_{5,0} - \tfrac{9625}{323}\mathrm{A}_{5,1} + \tfrac{88695}{1292}\mathrm{A}_{5,2} - \tfrac{25920}{323}\mathrm{A}_{5,3} + \tfrac{185220}{4199}\mathrm{A}_{5,4} - \tfrac{14917}{7752}\mathrm{A}_{6,0} + \tfrac{46975}{3876}\mathrm{A}_{6,1} - \tfrac{83025}{2584}\mathrm{A}_{6,2} \\ & + \tfrac{192600}{4199}\mathrm{A}_{6,3} - \tfrac{154350}{4199}\mathrm{A}_{6,4} + \tfrac{666792}{46189}\mathrm{A}_{6,5} + \tfrac{2761}{6783}\mathrm{A}_{7,0} - \tfrac{19300}{6783}\mathrm{A}_{7,1} + \tfrac{501525}{58786}\mathrm{A}_{7,2} - \tfrac{417600}{29393}\mathrm{A}_{7,3} + \tfrac{652680}{46189}\mathrm{A}_{7,4} \\ & - \tfrac{381024}{46189}\mathrm{A}_{7,5} + \tfrac{110250}{46189}\mathrm{A}_{7,6} - \tfrac{831}{18088}\mathrm{A}_{8,0} + \tfrac{4925}{13832}\mathrm{A}_{8,1} - \tfrac{564975}{470288}\mathrm{A}_{8,2} + \tfrac{43740}{19019}\mathrm{A}_{8,3} - \tfrac{6615}{2431}\mathrm{A}_{8,4} + \tfrac{186543}{92378}\mathrm{A}_{8,5} \\ & - \tfrac{165375}{184756}\mathrm{A}_{8,6} + \tfrac{9000}{46189}\mathrm{A}_{8,7} + \tfrac{4861}{2116296}\mathrm{A}_{9,0} - \tfrac{10475}{529074}\mathrm{A}_{9,1} + \tfrac{14985}{198968}\mathrm{A}_{9,2} - \tfrac{53520}{323323}\mathrm{A}_{9,3} + \tfrac{21315}{92378}\mathrm{A}_{9,4} - \tfrac{882}{4199}\mathrm{A}_{9,5} \\ & + \tfrac{875}{7106}\mathrm{A}_{9,6} - \tfrac{2000}{46189}\mathrm{A}_{9,7} + \tfrac{675}{92378}\mathrm{A}_{9,8} - \tfrac{671}{21162960}\mathrm{A}_{10,0} + \tfrac{7129}{23279256}\mathrm{A}_{10,1} - \tfrac{6849}{5173168}\mathrm{A}_{10,2} + \tfrac{99}{29393}\mathrm{A}_{10,3} - \tfrac{1029}{184756}\mathrm{A}_{10,4} \\ & + \tfrac{2877}{461890}\mathrm{A}_{10,5} - \tfrac{875}{184756}\mathrm{A}_{10,6} + \tfrac{10}{4199}\mathrm{A}_{10,7} - \tfrac{135}{184756}\mathrm{A}_{10,8} + \tfrac{5}{46189}\mathrm{A}_{10,9}, \end{aligned}$$

$$\begin{aligned} \mathrm{H}_{[24]} = {} & \mathrm{A}_{1,0} - \tfrac{11}{2}\mathrm{A}_{2,0} + \tfrac{432}{23}\mathrm{A}_{2,1} + \tfrac{905}{69}\mathrm{A}_{3,0} - \tfrac{1440}{23}\mathrm{A}_{3,1} + \tfrac{15972}{161}\mathrm{A}_{3,2} - \tfrac{1635}{92}\mathrm{A}_{4,0} + \tfrac{702}{7}\mathrm{A}_{4,1} - \tfrac{35937}{161}\mathrm{A}_{4,2} + \tfrac{665500}{3059}\mathrm{A}_{4,3} \\ & + \tfrac{12126}{805}\mathrm{A}_{5,0} - \tfrac{76896}{805}\mathrm{A}_{5,1} + \tfrac{3865224}{15295}\mathrm{A}_{5,2} - \tfrac{1064800}{3059}\mathrm{A}_{5,3} + \tfrac{24257475}{104006}\mathrm{A}_{5,4} - \tfrac{953}{115}\mathrm{A}_{6,0} + \tfrac{126376}{2185}\mathrm{A}_{6,1} - \tfrac{378004}{2185}\mathrm{A}_{6,2} \\ & + \tfrac{6355525}{22287}\mathrm{A}_{6,3} - \tfrac{8085825}{29716}\mathrm{A}_{6,4} + \tfrac{6899904}{52003}\mathrm{A}_{6,5} + \tfrac{45454}{15295}\mathrm{A}_{7,0} - \tfrac{345888}{15295}\mathrm{A}_{7,1} + \tfrac{19489833}{260015}\mathrm{A}_{7,2} - \tfrac{7320500}{52003}\mathrm{A}_{7,3} \\ & + \tfrac{118053045}{728042}\mathrm{A}_{7,4} - \tfrac{41399424}{364021}\mathrm{A}_{7,5} + \tfrac{4024944}{96577}\mathrm{A}_{7,6} - \tfrac{8315}{12236}\mathrm{A}_{8,0} + \tfrac{1168245}{208012}\mathrm{A}_{8,1} - \tfrac{8509083}{416024}\mathrm{A}_{8,2} + \tfrac{62523725}{1456084}\mathrm{A}_{8,3} \\ & - \tfrac{331518825}{5824336}\mathrm{A}_{8,4} + \tfrac{230715540}{4732273}\mathrm{A}_{8,5} - \tfrac{2515590}{96577}\mathrm{A}_{8,6} + \tfrac{705672}{96577}\mathrm{A}_{8,7} + \tfrac{176005}{1872108}\mathrm{A}_{9,0} - \tfrac{131564}{156009}\mathrm{A}_{9,1} + \tfrac{3674891}{1092063}\mathrm{A}_{9,2} \\ & - \tfrac{25688300}{3276189}\mathrm{A}_{9,3} + \tfrac{222509925}{18929092}\mathrm{A}_{9,4} - \tfrac{55582560}{4732273}\mathrm{A}_{9,5} + \tfrac{752136}{96577}\mathrm{A}_{9,6} - \tfrac{313632}{96577}\mathrm{A}_{9,7} + \tfrac{136125}{193154}\mathrm{A}_{9,8} - \tfrac{2339}{328440}\mathrm{A}_{10,0} \\ & + \tfrac{126393}{1820105}\mathrm{A}_{10,1} - \tfrac{1106061}{3640210}\mathrm{A}_{10,2} + \tfrac{1311035}{1670214}\mathrm{A}_{10,3} - \tfrac{50132115}{37858184}\mathrm{A}_{10,4} + \tfrac{2117016}{1391845}\mathrm{A}_{10,5} - \tfrac{30492}{25415}\mathrm{A}_{10,6} + \tfrac{307098}{482885}\mathrm{A}_{10,7} \\ & - \tfrac{81675}{386308}\mathrm{A}_{10,8} + \tfrac{24200}{676039}\mathrm{A}_{10,9} + \tfrac{58301}{240253860}\mathrm{A}_{11,0} - \tfrac{51684}{20021155}\mathrm{A}_{11,1} + \tfrac{588181}{47322730}\mathrm{A}_{11,2} - \tfrac{506990}{14196819}\mathrm{A}_{11,3} \\ & + \tfrac{98901}{1456084}\mathrm{A}_{11,4} - \tfrac{2119392}{23661365}\mathrm{A}_{11,5} + \tfrac{40194}{482885}\mathrm{A}_{11,6} - \tfrac{26136}{482885}\mathrm{A}_{11,7} + \tfrac{2475}{104006}\mathrm{A}_{11,8} - \tfrac{4400}{676039}\mathrm{A}_{11,9} + \tfrac{594}{676039}\mathrm{A}_{11,10} \\ & - \tfrac{6617}{2883046320}\mathrm{A}_{12,0} + \tfrac{83711}{3123300180}\mathrm{A}_{12,1} - \tfrac{81191}{567872760}\mathrm{A}_{12,2} + \tfrac{78419}{170361828}\mathrm{A}_{12,3} - \tfrac{75339}{75716368}\mathrm{A}_{12,4} + \tfrac{35937}{23661365}\mathrm{A}_{12,5} \\ & - \tfrac{1617}{965770}\mathrm{A}_{12,6} + \tfrac{4521}{3380195}\mathrm{A}_{12,7} - \tfrac{4125}{5408312}\mathrm{A}_{12,8} + \tfrac{605}{2028117}\mathrm{A}_{12,9} - \tfrac{99}{1352078}\mathrm{A}_{12,10} + \tfrac{6}{676039}\mathrm{A}_{12,11}. \end{aligned}$$

References

[1] J. Gans, D. Shalloway, Shadow mass and the relationship between velocity and momentum in symplectic numerical integration, Phys. Rev. E 61 (4) (2000) 4587–4592.

[2] E. Hairer, C. Lubich, G. Wanner, Geometric Numerical Integration, Springer Series in Computational Mathematics, vol. 31, Springer-Verlag, Berlin, 2002.
[3] R.D. Skeel, D.J. Hardy, Practical construction of modified Hamiltonians, SIAM J. Sci. Comput. 23 (4) (2001) 1172–1188.
[4] J.M. Borwein, R.M. Corless, Emerging tools for experimental mathematics, Am. Math. Monthly 106 (10) (1999) 889–909.
[5] J. Sanz-Serna, M. Calvo, Numerical Hamiltonian Problems, Chapman & Hall, London, 1994.
[6] G. Benettin, A. Giorgilli, On the Hamiltonian interpolation of near to the identity symplectic mappings with application to symplectic integration algorithms, J. Stat. Phys. 74 (1994) 1117–1143.
[7] B. Moore, S. Reich, Backward error analysis for multi-symplectic integration methods, Numer. Math. 95 (2003) 625–652.
[8] R.D. Engle, Interpolated modified Hamiltonians, Master's Thesis, University of Illinois at Urbana-Champaign, October 2003. Available from: http://bionum.cs.purdue.edu/Engl03.ps.
[9] J. Moser, Stable and Random Motions in Dynamical Systems, Princeton University Press, Princeton, NJ, 1973.
[10] L. Kalé, R. Skeel, R. Brunner, M. Bhandarkar, A. Gursoy, N. Krawetz, J. Phillips, A. Shinozaki, K. Varadarajan, K. Schulten, NAMD 2: Greater scalability for parallel molecular dynamics, J. Comput. Phys 151 (1) (1999) 283–312.